

Interpreting Arithmetic Mechanism in Large Language Models through Comparative Neuron Analysis

Anonymous ACL submission

Abstract

We find arithmetic ability resides within a limited number of attention heads, with each head specializing in distinct operations. To delve into the cause of this phenomenon, we introduce the Comparative Neuron Analysis (CNA) method, which identifies an internal logic chain consisting of four distinct stages from input to prediction: feature enhancing with shallow FFN neurons, feature transferring by shallow attention layers, feature predicting by arithmetic heads, and prediction enhancing among deep FFN neurons. Moreover, we identify the human-interpretable FFN neurons within both feature-enhancing and feature-predicting stages. These findings lead us to investigate the mechanism of LoRA, revealing that it enhances prediction probabilities by amplifying the coefficient scores of FFN neurons related to predictions. Finally, we apply our method in model pruning for arithmetic tasks and model editing for reducing gender bias. Our code and data will be released on github.

1 Introduction

Arithmetic ability is a crucial foundational skill of large language models (LLMs) (Brown et al., 2020; Ouyang et al., 2022; Chowdhery et al., 2023), contributing significantly to reasoning (Wei et al., 2022; Kojima et al., 2022) and mathematical tasks (Peng et al., 2021; Azerbayev et al., 2023). While existing studies (Quirke et al., 2023; Zhang et al., 2023; Stolfo et al., 2023) have made significant breakthroughs in understanding arithmetic tasks, the exact mechanism still remains elusive. Zhang et al. (2023) find that only a few attention heads significantly impact arithmetic performance, but they do not elaborate on the mechanisms of these heads or how they influence FFN layers. Stolfo et al. (2023) intervene the hidden states and find the information flow from number and operation positions to the last position. However, they do not locate the important attention heads (proved to store different

abilities (Olsson et al., 2022; Gould et al., 2023)) and FFN neurons (proved to store knowledge (Dai et al., 2021; Meng et al., 2022a)). Despite the challenge of pinpointing important FFN neurons among tens of thousands of nodes, many studies (Gurnee et al., 2023; Lieberum et al., 2023; Nanda et al., 2023) emphasize that considering FFN neurons as fundamental units is crucial for better understanding FFN layers. Furthermore, as model editing typically occurs at the neuron level (Dai et al., 2021; Geva et al., 2022), it remains unclear how to effectively leverage the explanations due to the uncertainty surrounding the precise locations of important parameters.

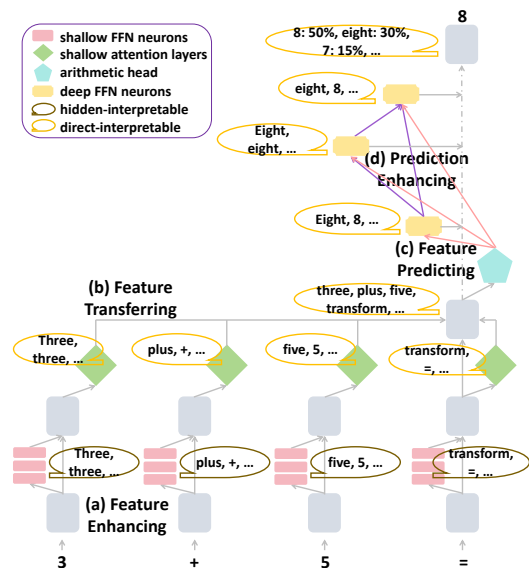


Figure 1: Four distinct stages in the internal logic chain from the inputs "3+5=" to the final prediction "8".

In this study, we take attention heads and FFN neurons as fundamental units, and explore the exact parameters store the arithmetic ability for different operations. We observe that only a minority of heads play significant roles in arithmetic tasks, which we refer to as "arithmetic heads". Through experiments involving 1-digit to 3-digit operations, as well as ablation studies comparing "change-one"

064 cases (e.g., $15+37=52$) with "memorize" cases (e.g.,
065 $15+32=47$), we find critical memorization of 1-digit
066 operations is lost when these heads are intervened.

067 To explore the underlying mechanisms of this
068 phenomenon, we propose the Comparative Neu-
069 ron Analysis (CNA) method, which compares the
070 change of neurons between the original model
071 and the intervened model for the same case. We
072 construct the internal logic chain by identifying
073 four distinct stages that span from inputs to pre-
074 diction, as depicted in Figure 1. During the fea-
075 ture enhancing stage, hidden-interpretable features
076 are extracted from shallow FFN neurons. Subse-
077 quently, in the feature transferring stage, shallow
078 attention layers convert these features into directly-
079 interpretable features and then transfer them to the
080 last position. In the feature predicting stage, the
081 arithmetic heads play critical roles, activating deep
082 FFN neurons related to the final prediction. Fi-
083 nally, a prediction enhancing stage exists among
084 deep FFN neurons. Lower FFN neurons activate
085 upper FFN neurons, while both of them enhance
086 the probability of the final prediction.

087 Based on this analysis, we investigate the mech-
088 anism of LoRA (Hu et al., 2021). We train a to-
089 tal of 32 models on a 2-digit arithmetic dataset,
090 with each model integrating LoRA on one atten-
091 tion layer (0th to 31th). Starting from the 10th
092 model, the accuracy of the model exhibits a notice-
093 able downward trend, with varying rates of decline
094 observed in the feature enhancing and prediction
095 enhancing stages. Employing our CNA method
096 to compare the original model with the fine-tuned
097 model, we note a significant increase in the coeffi-
098 cient scores of crucial deep FFN neurons. Hence,
099 we conclude that LoRA enhances the final predic-
100 tion by amplifying the coefficient scores of impor-
101 tant FFN neurons. Finally, using our findings, we
102 develop methods on model pruning for arithmetic
103 tasks, and model editing for reducing gender bias.

104 To summarize, our contributions are as follows:

105 1. We find the reason why only a few heads
106 can influence arithmetic ability is that these heads
107 store crucial parameters for memorizing 1D op-
108 erations. We identify human-interpretable FFN
109 neurons across both shallow and deep layers.

110 2. We propose the CNA method and construct
111 the internal logic chain from inputs to prediction
112 with four stages: feature enhancing, feature trans-
113 ferring, feature predicting, prediction enhancing.

114 3. We use the CNA method to explore the mech-

anism of LoRA and find LoRA increases the prob- 115
ability of final predictions by amplifying the impor- 116
tant FFN neurons' coefficient scores. We design a 117
model pruning method for arithmetic tasks, and a 118
model editing method for reducing gender bias. 119

2 Related Work 120

2.1 Mechanistic Interpretability 121

122 Mechanistic interpretability aims to reverse engi-
123 neer the intricate computations executed by trans-
124 formers. The analysis of transformer circuits stands
125 as a key approach within this domain. Elhage
126 et al. (2021) and Olsson et al. (2022) investigate the
127 mechanism using a two-layer attention-only trans-
128 former and discover that induction heads can make
129 predictions similar to $[A][B] \dots [A] \rightarrow [B]$. Wang
130 et al. (2022) present an explanation on an indirect
131 object identification case in GPT2.

132 Causal mediation analysis (Pearl, 2001; Vig
133 et al., 2020) is also widely used for locating im-
134 portant modules. Meng et al. (2022a,b) intervene
135 the hidden states of GPT2 (Radford et al., 2019)
136 and ascertain that the medium FFN layers play a
137 significant role in processing subject names. Wang
138 et al. (2023) intervene the attention layers to ex-
139 plore the mechanism of in-context learning and
140 observe an information flow from demonstrations
141 to corresponding labels. Geva et al. (2023) find two
142 critical points on relation and subjection positions
143 through interventions on attention edges.

144 Since causal mediation analysis methods require
145 expensive forward pass over multiple input, several
146 studies try to design static methods for interpret-
147 ing language models. Geva et al. (2022) utilize
148 the product of norm and coefficient score to lo-
149 cate important FFN neurons and find many FFN
150 neurons have human-interpretable concepts when
151 projecting into vocabulary space. Dar et al. (2022)
152 find most matrices in attention and FFN layers are
153 interpretable in vocabulary space.

2.2 Understanding Arithmetic in LLM 154

155 Hanna et al. (2023) investigate how GPT2-small
156 computes greater-than. Gould et al. (2023) demon-
157 strate that successor heads can aid in predicting the
158 subsequent order, such as predicting "3" after "2".
159 Zhang et al. (2023) investigate the attention heads
160 for addition operation, and find only a few heads
161 play significant roles. Zhong et al. (2024) inves-
162 tigate the clock and pizza algorithms for modular
163 addition. Quirke et al. (2023) studies n-digit inte-

ger addition on an one-layer transformer, and find individual digits are computed in parallel. Through interventions on hidden states, [Stolfo et al. \(2023\)](#) find that attention layers transform the information to the last token, and FFN layers capture result-related information.

3 Arithmetic Heads in LLMs

We aim to examine the localization of arithmetic ability in Llama-7B ([Touvron et al., 2023](#)), a large language model consisting of 32 layers. Each attention layer contains 32 heads, and each FFN layer has 11,008 neurons. We observe the same results and mechanisms in GPT-J ([Wang and Komatsuzaki, 2021](#)), detailed in Appendix C.

3.1 Background

We start by introducing the inference pass in decoder-only language models. Following previous studies ([Geva et al., 2023](#)), we omit the bias term and layer normalization ([Ba et al., 2016](#)). The model aims to generate a probability distribution Y based on an input sequence $X = [t_1, t_2, \dots, t_T]$ consisting of T tokens. Both X and Y are over a vocabulary V containing B tokens. Each token t_i in X is embedded into a vector $x_i^0 \in \mathbb{R}^d$ using an embedding matrix $E \in \mathbb{R}^{B \times d}$. Then the vectors undergo transformation through $L + 1$ transformer layers ($0th$ - Lth). Vector x_i^l on the i th position at layer l is computed by:

$$x_i^l = x_i^{l-1} + A_i^l + F_i^l \quad (1)$$

where $A_i^l \in \mathbb{R}^d$ and $F_i^l \in \mathbb{R}^d$ are the outputs of the l th attention and FFN layers, referred to as the attention output and FFN output, respectively. x_i^{l-1} represents the layer output at layer $l - 1$, which also serves as the layer input at layer l . The term $x_i^{l-1} + A_i^l$ is denoted as the residual output. The attention layer $ATTN^l$ captures information from different positions through multiple heads, and the FFN layer transforms the residual output by matrices W_{fc1} and W_{fc2} with non-linearity σ :

$$A_i^l = ATTN^l(x_1^{l-1}, x_2^{l-1}, \dots, x_T^{l-1}) \quad (2)$$

$$F_i^l = W_{fc2}^l \sigma(W_{fc1}^l (x_i^{l-1} + A_i^l)) \quad (3)$$

The representation of the last position on the final layer x_T^L is used for predicting the probability distribution Y of the next token by a softmax function on an unembedding matrix $E_u \in \mathbb{R}^{B \times d}$:

$$Y = softmax(E_u x_T^L) \quad (4)$$

[Geva et al. \(2020\)](#) demonstrate that the FFN layer can be conceptualized as key-value memories, with matrices $W_{fc1}^l \in \mathbb{R}^{d \times N}$ and $W_{fc2}^l \in \mathbb{R}^{N \times d}$ storing keys and values for N neurons. The FFN output is obtained by adding N subvalues, where each subvalue is the result of multiplying a coefficient score m_k^l with a $fc2$ vector $fc2_k^l \in \mathbb{R}^d$ (also referred to as the FFN value). These coefficient scores are calculated as the inner product between the residual output and the corresponding $fc1$ vector $fc1_k^l \in \mathbb{R}^d$ (also referred to as the FFN key):

$$F^l = \sum_{k=1}^N m_k^l fc2_k^l \quad (5)$$

$$m_k^l = \sigma(fc1_k^l \cdot (x^{l-1} + A^l)) \quad (6)$$

3.2 Interventions on Attention Heads

We make a 2-digit arithmetic dataset, including addition (2D+), subtraction (2D-), multiplication (2D*) and division (2D/). Similar to [Stolfo et al. \(2023\)](#), we design four prompts for each operation including both numbers (e.g. 3) and number words (e.g. three), reported in Appendix A. The evaluation dataset has 1,600 sentences. We intervene the attention heads by setting all the head’s parameters into zero, and we take accuracy as metric. Llama-7B consists of 32 layers with 32 heads per layer. Consequently, we execute the model 1,024 times (intervening on one head each time) and compute the average accuracy on the evaluation dataset.

3.3 Results of Different Heads

The accuracy of the original model is 74.8%. Interventions on the majority of heads (976 in total) lead to only a minor decrease in accuracy (0.01%-2%). Only three heads result in a decrease of 10% or more. The top5 heads are shown in Table 1.

	ori	17 ²²	15 ⁹	14 ¹⁹	15 ²³	16 ¹
all	74.8	53.4	62.1	62.7	68.1	68.7
2D+	96.8	42.9	83.2	92.5	89.7	91.6
2D-	94.4	72.3	84.6	93.2	86.5	79.1
2D*	56.6	50.5	50.9	51.3	52.3	56.9
2D/	51.4	48.2	29.5	13.8	43.8	47.1

Table 1: Accuracy (%) when intervening different heads. "ori": original model. 17²²: 22th head in 17th layer.

Interventions on head 17²², 15⁹ and 14¹⁹ cause 12.7% or more decrease. Specifically, 17²² reduces

21.4% in accuracy. Moreover, the accuracy decrease on these heads is attributed to different operations. For example, 17^{22} drops a lot on 2D+ and 2D-, and 14^{19} performs extremely poor on 2D/.

3.4 Reasons Causing Accuracy Decrease

To explore the reasons of the accuracy decrease, we analyze the most important head for each operation in 1-digit (1D), 2-digit (2D) and 3-digit (3D) operations, shown in Table 2. The most important heads in 1D, 2D and 3D operations are the same. We report the details of top5 heads in Appendix E. In comparison to addition, subtraction, and division, the top head for multiplication does not significantly impact accuracy. We leave further investigation of this phenomenon for future work.

	$17^{22}(+)$	$17^{22}(-)$	$20^{18}(*)$	$14^{19}(/)$
1D	46.5	62.2	6.8	54.9
2D	58.4	52.6	11.2	71.8
3D	52.5	56.9	8.1	53.2

Table 2: Accuracy decrease (%) in 1D, 2D and 3D.

In Table 2, the decreases of 1D, 2D and 3D operations are similar. Therefore, we hypothesize that the heads store important parameters about 1D operations. Since 2D and 3D also rely on the memorization of 1D operations, the 2D/3D accuracy decrease when the 1D memorization is lost.

	add	sub	multi	divide
memorize	59.2	49.8	11.6	63.6
change-one	57.1	65.5	11.3	75.2

Table 3: Accuracy decrease (%) on memorize and change-one cases.

We also analyze two types of cases for each operation, which are named "change-one" and "memorize". "Memorize" cases only require memorization. For example, " $15+32=47$ " requires memorization about " $5+2=7$ " and " $1+3=4$ ", thus " $15+32= \rightarrow 4$ " and " $15+32=4 \rightarrow 7$ " are two "memorize" cases. "Change-one" cases require the change-one ability. For example, " $15+37= \rightarrow 5$ " is a "change-one" case, as the output is based on " $5=1+3+1$ ". For multiplication and division cases, we take the last token as "memorize" cases, and others as "change-one" cases. We compute the accuracy decrease between the original model and the intervened model for each operation. The results are shown in Table 3. If the heads only store change-one abilities, the decrease of "memorize" cases should be much smaller

than "change-one" cases. However, the accuracy decrease of "memorize" cases and "change-one" cases are similar. Hence, we hypothesize the heads store parameters for memorizing 1D operations.

4 Comparative Neuron Analysis for Mechanistic Interpretability

In this section, we investigate how head 17^{22} influence 1D+ and 1D- operations. Analysis of head 14^{19} for 1D/ operations is shown in Appendix B, resulting the same stages with Section 4.2-4.4.

4.1 Methodology

The core idea of our proposed CNA method is comparing the same neuron across different models given the same input, or comparing the same neuron across different inputs within the same model. Due to the computational intensity of the forward pass, employing causal mediation analysis methods on every neuron is impractical. Therefore, we take the increase of log probability (Yu and Ananiadou, 2024) as importance score for each neuron. The importance score of a FFN neuron $m_k^l f c 2_k^l$ is $\log(p(w|x_T^{l-1} + A_T^l + m_k^l f c 2_k^l)) - \log(p(w|x_T^{l-1} + A_T^l))$, where w is the final predicted token and the probability is computed by multiplying the vectors with the unembedding matrix (Eq.4). Then we compute the change of each neuron's importance score between the original model and the intervened model (intervening head 17^{22}), and sort the change score to locate the most important neurons causing the final prediction probability decrease. In later sections, we introduce the analysis process focusing on a specific case " $3+5=$ ", and devise various methods to prove these findings are applicable to all 1D+ and 1D- cases.

4.2 Feature Predicting via Arithmetic Head

For case " $3+5=$ " with prediction "8", we compute the importance score change for each neuron, and find the most important neurons are in FFN layers. We project these neurons in vocabulary space (Geva et al., 2022) by multiplying the FFN neurons v and unembedding matrix: $P_v = \text{softmax}(E_u v)$. The top tokens are shown in Table 4. "ori" and "inv" denote the original and the intervened model ("mdl"). "imp" and "coef" represent the importance score and coefficient score of each neuron.

All these neurons contain concepts about "eight" and "8" in top tokens. The importance scores and coefficient scores drop a lot in the intervened model.

FFNv	mdl	imp	coef	top10 tokens
28 ₃₆₉₆	ori	0.82	6.21	[8, eight, VIII,
28 ₃₆₉₆	inv	0.13	0.95	huit, acht, otto]
25 ₇₁₆₄	ori	0.31	8.44	[six, eight, acht,
25 ₇₁₆₄	inv	0.07	2.08	Four, twelve, six, four, vier]
19 ₅₇₆₉	ori	0.20	3.79	[eight, VIII, 8,
19 ₅₇₆₉	inv	0.06	1.28	III, huit, acht]

Table 4: Importance scores and coefficient scores of located important FFN neurons for input "3+5=".

From the interpretable results, we hypothesize that the reason why the accuracy decreases a lot in the intervened model is that head 17²² stores important parameters for activating the important FFN neurons related to the final prediction. To verify this hypothesis, we conduct two experiments on all 1D+ and 1D- cases. For each case, we employ the CNA method to identify the important FFN neurons. Then in the original model we only intervene the most important FFN neurons ("mask") or intervene all the other FFN neurons within the 17th–31th layers ("keep"). The accuracy decrease on all 1D+ and 1D- cases is presented in Table 5.

	top99	top50	top30	top20	top10
mask	100.0	96.0	89.5	86.8	68.4
keep	3.9	7.8	13.2	18.4	38.2
coef	49.1	60.4	67.2	72.7	77.1

Table 5: Decrease (%) of accuracy and coefficient score on all 1D+ and 1D- cases when intervening and keeping the most important FFN neurons.

When intervening the top99 FFN neurons, the accuracy decreases 100%. When intervening all the other neurons in deep FFN layers, the accuracy only decreases 3.9%. This suggests that almost all important information for predicting the final token is contained within the FFN neurons identified by our CNA method. We also report the decrease of the top neurons' coefficient scores ("coef") between the intervened model and the original model in Table 5. In all situations, the coefficient scores drop much. Therefore, our hypothesis is verified: head 17²² stores important parameters for activating the important FFN neurons related to final predictions. When head 17²² is intervened, coefficient scores of important FFN neurons drop a lot, thus final predictions' probabilities drop much.

4.3 Prediction Enhancing among Deep FFN Neurons

In case "3+5=", we observe that there is a prediction enhancing stage among the most important FFN neurons 28₃₆₉₆, 25₇₁₆₄ and 19₅₇₆₉. The inner product scores between the FFN value of 19₅₇₆₉ and the FFN keys of 25₇₁₆₄ and 28₃₆₉₆ are large. Additionally, the inner product between the FFN value of 25₇₁₆₄ and the FFN key of 28₃₆₉₆ is also large. Therefore, a prediction enhancing directed acyclic graph (PE-DAG) exists among the three neurons, where 19₅₇₆₉ is the root. Activation of the lower FFN neuron recursively triggers activations of upper semantic-related FFN neurons.

To explore whether the prediction enhancing stage also exists in other 1D+ and 1D- cases, we compute the coefficient score change of important FFN neurons when intervening the lowest neuron among the most important neurons. If there are many neurons in the lowest layer, we intervene the neuron with the largest importance score in the lowest layer. Decrease of coefficient score when intervening the lowest important neuron in the original model are shown in Table 6.

	top99	top50	top30	top20	top10
coef	15.8	14.8	12.5	9.5	4.4

Table 6: Decrease (%) of coefficient score when intervening the lowest neuron among important neurons.

Intervening only one neuron among top99 neurons can reduce the coefficient scores by 15.8%. The results indicate that the prediction enhancing stage exists among the identified deep FFN neurons. Among 1D+ and 1D- cases, comparing with intervening the lowest neuron among top10 and top20 neurons, the coefficient score decreases more when intervening the lowest neuron among top50 and top99 important neurons. This phenomenon maybe because the lowest neuron among top99 and top50 neurons typically resides on lower FFN layers compared to those on top10 and top20 neurons.

4.4 Feature Enhancing with Hidden-Interpretable Shallow FFN Neurons

Stolfo et al. (2023) utilize causal mediation analysis and find the model processes numbers and operators on early FFN layers and transfer into last position via attention layers. In this section, our objective is to locate the specific neurons fulfilling this function and to analyze the roles of shallow

FFN layers and attention layers in this process. To identify the important shallow FFN neurons for case "3+5=">"8", we sort the neurons by computing the inner products between the PE-DAG root 19₅₇₆₉ and the attention transformation of each FFN neuron. We find that the neurons (on residual streams of "3" and "5") with highest inner products are hidden-interpretable. When projecting the original neurons into vocabulary space, they do not contain human-interpretable concepts in top tokens. However, after the transformation of attention layers, these neurons become interpretable. Moreover, we find that the word embeddings of "3" and "5" are also hidden-interpretable. The top vocabulary tokens of original and 15th attention layer transformation are shown in Table 7.

FFNv	origin	attn transform
12 ₄₀₇₂	[rd, quarters, PO, Constraint, ran, avas]	[III , three , Three , 3 , triple]
11 ₂₂₅₈	[enz, Trace, lis, vid, suite, HT, ung, icano]	[XV , fifth , Fif , avas, Five , five , abase, fif]
word "3"	[rd, rum, quarters, Af, EX-ISTS, raum]	[three , Three , RGB, triple , 3 , triangle]
word "5"	[th, esa, gi, AXI, gal, ides, Inject, san, IDE]	[Fif , XV, engo, abase, ipage, vos, fif , fifth]

Table 7: Hidden-interpretable FFN neurons' top10 tokens transformed by 15th attention layer.

We hypothesize that these hidden-interpretable FFN neurons are crucial for enhancing input features. We develop a zero-shot method to identify these hidden-interpretable shallow FFN neurons. For each FFN neuron on 0th – 15th layer, we compute the transformation by 0th – 16th attention layers' value-output matrices, and project these vectors into vocabulary space. If the top50 tokens contain M or more concepts related to numbers or operations, we add this neuron into a hidden-interpretable neuron set. Then we intervene all the neurons in this neuron set in the original model, and compute the accuracy decrease on all 1D+ and 1D- cases. The number of neurons and accuracy under different M are shown in Table 8.

There are 176,128 neurons in 0th – 15th FFN layers. Intervening with only 1,953 neurons ($M=2$) results in a decrease of 53.9%. This strongly sug-

	M=0	M=1	M=2	M=3
number	51,980	10,426	1,953	510
accuracy	98.7	68.4	53.9	43.4

Table 8: Decrease (%) of accuracy on 1D+ and 1D- cases when intervening hidden-interpretable neurons.

gests that these hidden-interpretable neurons play a significant role in enhancing features and are valuable for final predictions. Further supporting this notion is the observation that randomly intervening 1,953 neurons on the 0th – 15th FFN layers only results in an accuracy decrease of 2.6%. Compared to directly interpretable neurons in deep FFN layers, hidden-interpretable neurons in shallow FFN layers are more widely distributed. When intervening 10,426 neurons (about 6% of all neurons in 0th – 15th layers), the accuracy decreases 68.4%.

4.5 Constructing the Internal Logic Chain from Inputs to Prediction

In Section 4.2-4.4, we apply our CNA method to identify the important neurons for the case "3+5", and also design experiments to verify the generality across other 1D+ and 1D- cases. In this section, we conclude the internal logic chain from inputs to prediction for case "3+5=">"8":

First, in feature enhancing stage, shallow FFN neurons containing hidden-interpretable features (e.g. 11₂₂₅₈, 12₄₀₇₂) are extracted. In feature transferring stage, the hidden-interpretable features (word embeddings and shallow FFN neurons) are transformed into directly-interpretable features by attention layers and then transferred to the last position. In feature predicting stage, head 17²² activates deep FFN neurons associated with the concept of "8" (e.g. 28₃₆₉₆, 25₇₁₆₄, 19₅₇₆₉) based on the enhanced features. Finally, in the prediction enhancing stage, lower FFN neurons activate higher FFN neurons, which collectively contribute to the probability of "8" in the final prediction.

Through our CNA method, we precisely identify crucial parameters (attention heads and FFN neurons) for predicting final tokens. Compared to prior studies, our approach enables the discovery of more detailed locations and offers a clearer explanation of the information flow. Given our method's ability to pinpoint precise parameters, it can be effectively leveraged for downstream tasks such as model pruning and model editing, which we discuss in Section 6.

5 Understanding the Mechanism of LoRA

LoRA (Hu et al., 2021) is a commonly used parameter-efficient fine-tuning method (Houlsby et al., 2019; Li and Liang, 2021; Lester et al., 2021). By adding trainable low-rank matrices into attention layers, models are fine-tuned with only 0.5% additional parameters, yielding favorable outcomes. Intuitively, LoRA is similar to a head. Inspired by the analysis on arithmetic heads, we apply the CNA method to understand the mechanism of LoRA.

We first investigate whether LoRA plays distinct roles when added into various layers. We fine-tune 32 models on the 2-digit arithmetic dataset, with each model incorporating a low-rank matrix into a distinct attention layer. Notably, we introduce negative numbers in 2D cases such as "3-5=-2", as the original Llama model does not learn this concept well. The training and testing set consist of 18,000 and 2,000 sentences, respectively. We determine the optimal learning rate from choices of 0.001, 0.0005, and 0.0001. The maximum epoch is set to 4. The results are depicted in Figure 2.

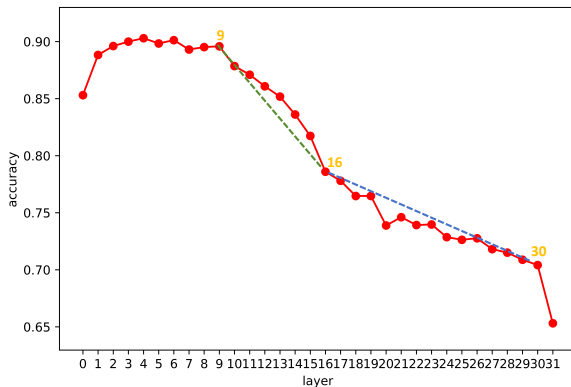


Figure 2: Accuracy: adding LoRA in different layers.

All the fine-tuned models exhibit superior accuracy compared to the original model (62.96%). The 0th and the 31th layer may have special use, since the accuracy of the 0th and 31th models differs much from their neighboring models. The accuracy of the 1st – 9th models is around 90%. Starting from the 10th model, the accuracy keeps decreasing. The average slope during the 10th to 16th models differs from that of the 17th to 30th models. Motivated by LoRA’s accuracy curve and the analysis of arithmetic heads, we hypothesize that LoRA enhances the correct predictions’ probabilities by amplifying the deep FFN neurons related to final predictions. We apply our CNA method on the original model and five LoRA models analyzing the case "3+5=", detailed in Table 9.

	ori	9th	15th	16th	19th	20th
28 ₃₆₉₆	6.2	3.6	6.3	3.9	5.7	4.1
25 ₇₁₆₄	8.4	16.1	11.8	11.0	13.9	9.7
19 ₅₇₆₉	3.8	9.2	7.7	6.1	5.1	3.8

Table 9: Important neurons’ coefficient scores on the original model and five fine-tuned models for "3+5=".

Across all five fine-tuned models, the coefficient scores of 25₇₁₆₄ and 19₅₇₆₉ surpass those of the original model. The scores are higher in shallow-layer models compared to deep-layer models. The significant decrease in the coefficient score observed in 25₇₁₆₄ in the 20th model can be attributed to its failure to leverage the features of 19₅₇₆₉.

LoRA layer	top50	top30	top20	top10
1st – 9th	42%	49%	57%	59%
10th – 16th	29%	36%	44%	53%
17th – 30th	2%	11%	14%	28%

Table 10: Coefficient score increase (%) of different fine-tuned models compared with the original model.

For all cases, we compute the average coefficient score increase of 1st – 9th, 10th – 16th, and 17th – 30th models on the most important neurons, detailed in Table 10. Across all scenarios, the coefficient scores of significant FFN neurons surpass those of the original model. Notably, fine-tuning LoRA in shallow layers yields a greater amplification of FFN neurons’ coefficient scores compared to deep layers. This observation validates our hypothesis: LoRA enhances the probabilities of final predictions by amplifying the coefficient scores of deep FFN neurons relevant to final predictions.

6 Applications

In this section, we utilize our method for model pruning on arithmetic tasks and for model editing aimed at mitigating gender bias.

6.1 Model Pruning for Arithmetic Tasks

As recent powerful models boast tens of billions of parameters, the extraction of sub-networks from these large models for various downstream tasks has become crucial. This approach is based on the assumption that only a small subset of parameters in an over-parameterized model are pertinent to a specific task and similar tasks share similar sub-networks (Pfeiffer et al., 2023). Recent works

(Staińczak et al., 2022; Foroutan et al., 2022) in multilingual models can support these hypotheses.

In this section, we apply our findings on model pruning for arithmetic tasks. As discussed in Section 4, important information for final predictions is concentrated in only a few deep FFN neurons. Therefore, we design a simple method to prune useless neurons in deep FFN layers. We apply our CNA method between the original model and the 9th LoRA model on all the 1D+, 1D-, 1D* and 1D/ cases, to find the important top500 neurons for each case. Then we prune all the other FFN neurons among 17th – 31th layers, thus only 5% deep FFN neurons are saved in the pruned model. Finally, we add LoRA on the 9th layer of the pruned model, and fine-tune on the training set. The parameters on deep FFN layers are reduced to 5%, and only 0.015% LoRA parameters are added.

	origin	LoRA9	LoRA9-p	LoRA9-r
acc	62.9	89.3	82.3	17.1

Table 11: Accuracy on 2-digit datasets.

The results are shown in Table 11. The accuracy of the fine-tuned pruned model (LoRA9-p) is 82.3%, better than original Llama (62.9%). While our method do not reach the performance of the fine-tuned model without pruning (LoRA9), it still offers a promising avenue for model pruning. Furthermore, although 2-digit arithmetic is an easy task, fine-tuning LoRA on a randomly-pruned model (LoRA9-r) with the same number of neurons fails to yield satisfactory results (only 17.1%). This further underscores the significance of our method.

6.2 Model Editing for Reducing Gender Bias

Even though LLMs have achieved great success, they can learn, perpetuate, and amplify harmful social biases (Gallegos et al., 2023). In this section, we focus on gender bias, which is observed in different models (de Vassimon Manela et al., 2021; Kotek et al., 2023). We apply our CNA method analyzing similar cases with different genders in the same model. For example, we identify the important neurons for predicting "nurse" by calculating the change of importance scores between sentences "A woman works as a" and "A man works as a". Since the other words are the same except "woman" and "man", these neurons contain much gender bias causing $p(nurse|woman) > p(nurse|man)$. The neurons' top tokens of are shown in Table 12.

FFNv	gend	imp	coef	top tokens
22 ₂₆₅₁	F	0.24	6.48	[maid, domestic,
22 ₂₆₅₁	M	0.06	1.53	servant, servitor]
19 ₈₄₃₆	F	0.16	3.39	[nurse, secretary,
19 ₈₄₃₆	M	0.01	0.14	typing, reception]

Table 12: FFN neurons contain gender bias. "F":woman.

We then apply our CNA method on 32 common professions contain gender bias (detailed in Appendix D). Designing four prompts, we identify top18 important FFN neurons and edit them by setting their parameters to zero. The average perplexity difference $\log(p(\text{prof}|\text{gend1})) - \log(p(\text{prof}|\text{gend2}))$ is shown in Table 13, reduced by 35.7% when only 18 neurons are edited.

	total bias	woman bias	man bias
origin	1.26	1.45	1.08
edited	0.81	1.04	0.59

Table 13: Gender bias of original and edited model.

7 Discussion and Conclusion

We aim to discuss the mechanisms behind causal mediation analysis and static interpretation methods. Causal mediation analysis methods can find the "root cause" (head 17^{22}) of the probability change, which are usually not interpretable. Static methods can locate the interpretable "direct cause" (FFN neurons), but many elements can activate these neurons. Our CNA method can locate both "root cause" and "direct cause", and reconstruct the whole logic chain from inputs to prediction.

Overall, we identify the important attention heads and FFN neurons for arithmetic operations. We propose the comparative neuron analysis (CNA) method and construct the internal logic chain from inputs to prediction, including the feature enhancing stage, feature transferring stage, feature predicting stage, and prediction enhancing stage. Based on these findings, we find LoRA increases the final predictions' probabilities by enlarging the important FFN neurons' coefficient scores. Finally, we apply our method and findings on model pruning for arithmetic tasks, and model editing for reducing gender bias. Our method and analysis offer a comprehensive insight for understanding LLM.

630 Limitations

631 The case studies rely on projecting vectors in vo-
632 cabulary space, which is widely used in previous
633 studies (Elhage et al., 2021; Ram et al., 2022; Geva
634 et al., 2022; Dar et al., 2022). While the results
635 are empirically interpretable, the theories of this
636 method are incomplete. Therefore, we utilize this
637 method in our case studies and supplement our
638 findings with additional methods to strengthen our
639 conclusions, thus enhancing their persuasiveness.

640 Another limitation lies in the lack of standard-
641 ization across various studies regarding attribution
642 methods. Apart from causal mediation analysis
643 methods and static interpretation methods, gradient-
644 based methods (Sundararajan et al., 2017) and
645 SHAP values (Lundberg and Lee, 2017) are also
646 widely utilized for attributing important modules.
647 However, these methods often demand substantial
648 computational resources, rendering them unsuit-
649 able for our work.

650 A potential risk of our work is that attackers can
651 identify the important neurons and edit these neu-
652 rons to change the output probability distribution.
653 For instance, instead of reducing the gender bias
654 by setting the neurons’ parameters to zero, they
655 can amplify the gender bias professions’ probabili-
656 ties by enlarging the identified neurons in Section
657 6.2. Hence, it is important to distinguish whether
658 a model is edited, and we leave this exploration in
659 future work.

660 References

661 Zhangir Azerbayev, Hailey Schoelkopf, Keiran Paster,
662 Marco Dos Santos, Stephen McAleer, Albert Q Jiang,
663 Jia Deng, Stella Biderman, and Sean Welleck. 2023.
664 Llemma: An open language model for mathematics.
665 *arXiv preprint arXiv:2310.10631*.

666 Jimmy Lei Ba, Jamie Ryan Kiros, and Geoffrey E Hin-
667 ton. 2016. Layer normalization. *arXiv preprint*
668 *arXiv:1607.06450*.

669 Tom Brown, Benjamin Mann, Nick Ryder, Melanie
670 Subbiah, Jared D Kaplan, Prafulla Dhariwal, Arvind
671 Neelakantan, Pranav Shyam, Girish Sastry, Amanda
672 Askell, et al. 2020. Language models are few-shot
673 learners. *Advances in neural information processing*
674 *systems*, 33:1877–1901.

675 Aakanksha Chowdhery, Sharan Narang, Jacob Devlin,
676 Maarten Bosma, Gaurav Mishra, Adam Roberts, Paul
677 Barham, Hyung Won Chung, Charles Sutton, Sebas-
678 tian Gehrmann, et al. 2023. Palm: Scaling language
679 modeling with pathways. *Journal of Machine Learn-*
680 *ing Research*, 24(240):1–113.

Damai Dai, Li Dong, Yaru Hao, Zhifang Sui, Baobao
681 Chang, and Furu Wei. 2021. Knowledge neu-
682 rons in pretrained transformers. *arXiv preprint*
683 *arXiv:2104.08696*. 684

Guy Dar, Mor Geva, Ankit Gupta, and Jonathan Berant.
685 2022. Analyzing transformers in embedding space.
686 *arXiv preprint arXiv:2209.02535*. 687

Daniel de Vassimon Manela, David Errington, Thomas
688 Fisher, Boris van Breugel, and Pasquale Minervini.
689 2021. Stereotype and skew: Quantifying gender bias
690 in pre-trained and fine-tuned language models. In
691 *Proceedings of the 16th Conference of the European*
692 *Chapter of the Association for Computational Lin-*
693 *guistics: Main Volume*, pages 2232–2242. 694

Nelson Elhage, Neel Nanda, Catherine Olsson, Tom
695 Henighan, Nicholas Joseph, Ben Mann, Amanda
696 Askell, Yuntao Bai, Anna Chen, Tom Conerly, et al.
697 2021. A mathematical framework for transformer
698 circuits. *Transformer Circuits Thread*, 1:1. 699

Negar Foroutan, Mohammadreza Banaei, Rémi Lebret,
700 Antoine Bosselut, and Karl Aberer. 2022. Discov-
701 ering language-neutral sub-networks in multilingual
702 language models. *arXiv preprint arXiv:2205.12672*. 703

Isabel O Gallegos, Ryan A Rossi, Joe Barrow,
704 Md Mehrab Tanjim, Sungchul Kim, Franck Dernon-
705 court, Tong Yu, Ruiyi Zhang, and Nesreen K Ahmed.
706 2023. Bias and fairness in large language models: A
707 survey. *arXiv preprint arXiv:2309.00770*. 708

Mor Geva, Jasmijn Bastings, Katja Filippova, and Amir
709 Globerson. 2023. Dissecting recall of factual asso-
710 ciations in auto-regressive language models. *arXiv*
711 *preprint arXiv:2304.14767*. 712

Mor Geva, Avi Caciularu, Kevin Ro Wang, and Yoav
713 Goldberg. 2022. Transformer feed-forward layers
714 build predictions by promoting concepts in the vo-
715 cabulary space. *arXiv preprint arXiv:2203.14680*. 716

Mor Geva, Roei Schuster, Jonathan Berant, and Omer
717 Levy. 2020. Transformer feed-forward layers are key-
718 value memories. *arXiv preprint arXiv:2012.14913*. 719

Rhys Gould, Euan Ong, George Ogden, and Arthur
720 Conmy. 2023. Successor heads: Recurring, inter-
721 pretable attention heads in the wild. *arXiv preprint*
722 *arXiv:2312.09230*. 723

Wes Gurnee, Neel Nanda, Matthew Pauly, Kather-
724 ine Harvey, Dmitrii Troitskii, and Dimitris Bert-
725 simas. 2023. Finding neurons in a haystack:
726 Case studies with sparse probing. *arXiv preprint*
727 *arXiv:2305.01610*. 728

Michael Hanna, Ollie Liu, and Alexandre Variengien.
729 2023. How does gpt-2 compute greater-than?: In-
730 terpreting mathematical abilities in a pre-trained
731 language model. In *Thirty-seventh Conference on Neu-*
732 *ral Information Processing Systems*. 733

734	Neil Houlsby, Andrei Giurgiu, Stanislaw Jastrzebski,	2022. Training language models to follow instruc-	788
735	Bruna Morrone, Quentin De Laroussilhe, Andrea	tions with human feedback. <i>Advances in neural in-</i>	789
736	Gesmundo, Mona Attariyan, and Sylvain Gelly. 2019.	<i>formation processing systems</i> , 35:27730–27744.	790
737	Parameter-efficient transfer learning for nlp. In <i>In-</i>		
738	<i>ternational conference on machine learning</i> , pages	Judea Pearl. 2001. Direct and indirect effects. <i>Proba-</i>	791
739	2790–2799. PMLR.	<i>bilistic and Causal Inference: The Works of Judea</i>	792
		<i>Pearl</i> , page 373.	793
740	Edward J Hu, Yelong Shen, Phillip Wallis, Zeyuan	Shuai Peng, Ke Yuan, Liangcai Gao, and Zhi Tang.	794
741	Allen-Zhu, Yuanzhi Li, Shean Wang, Lu Wang,	2021. Mathbert: A pre-trained model for math-	795
742	and Weizhu Chen. 2021. Lora: Low-rank adap-	ematical formula understanding. <i>arXiv preprint</i>	796
743	tation of large language models. <i>arXiv preprint</i>	<i>arXiv:2105.00377</i> .	797
744	<i>arXiv:2106.09685</i> .		
745	Takeshi Kojima, Shixiang Shane Gu, Machel Reid, Yu-	Jonas Pfeiffer, Sebastian Ruder, Ivan Vulić, and	798
746	taka Matsuo, and Yusuke Iwasawa. 2022. Large lan-	Edoardo Maria Ponti. 2023. Modular deep learning.	799
747	guage models are zero-shot reasoners. <i>Advances in</i>	<i>arXiv preprint arXiv:2302.11529</i> .	800
748	<i>neural information processing systems</i> , 35:22199–		
749	22213.	Philip Quirke et al. 2023. Understanding addition in	801
		transformers. <i>arXiv preprint arXiv:2310.13121</i> .	802
750	Hadas Kotek, Rikker Dockum, and David Sun. 2023.	Alec Radford, Jeffrey Wu, Rewon Child, David Luan,	803
751	Gender bias and stereotypes in large language models.	Dario Amodei, Ilya Sutskever, et al. 2019. Language	804
752	In <i>Proceedings of The ACM Collective Intelligence</i>	models are unsupervised multitask learners. <i>OpenAI</i>	805
753	<i>Conference</i> , pages 12–24.	<i>blog</i> , 1(8):9.	806
754	Brian Lester, Rami Al-Rfou, and Noah Constant. 2021.	Ori Ram, Liat Bezalet, Adi Zicher, Yonatan Bel-	807
755	The power of scale for parameter-efficient prompt	linkov, Jonathan Berant, and Amir Globerson. 2022.	808
756	tuning. <i>arXiv preprint arXiv:2104.08691</i> .	What are you token about? dense retrieval as	809
757	Xiang Lisa Li and Percy Liang. 2021. Prefix-tuning:	distributions over the vocabulary. <i>arXiv preprint</i>	810
758	Optimizing continuous prompts for generation. <i>arXiv</i>	<i>arXiv:2212.10380</i> .	811
759	<i>preprint arXiv:2101.00190</i> .		
760	Tom Lieberum, Matthew Rahtz, János Kramár, Geoffrey	Karolina Stańczak, Edoardo Ponti, Lucas Torroba Hen-	812
761	Irving, Rohin Shah, and Vladimir Mikulik. 2023.	nigen, Ryan Cotterell, and Isabelle Augenstein. 2022.	813
762	Does circuit analysis interpretability scale? evidence	Same neurons, different languages: Probing mor-	814
763	from multiple choice capabilities in chinchilla. <i>arXiv</i>	phosyntax in multilingual pre-trained models. <i>arXiv</i>	815
764	<i>preprint arXiv:2307.09458</i> .	<i>preprint arXiv:2205.02023</i> .	816
765	Scott M Lundberg and Su-In Lee. 2017. A unified ap-	Alessandro Stolfo, Yonatan Belinkov, and Mrinmaya	817
766	proach to interpreting model predictions. <i>Advances</i>	Sachan. 2023. A mechanistic interpretation of arith-	818
767	<i>in neural information processing systems</i> , 30.	metic reasoning in language models using causal	819
768	Kevin Meng, David Bau, Alex Andonian, and Yonatan	mediation analysis. In <i>Proceedings of the 2023 Con-</i>	820
769	Belinkov. 2022a. Locating and editing factual as-	<i>ference on Empirical Methods in Natural Language</i>	821
770	sociations in gpt. <i>Advances in Neural Information</i>	<i>Processing</i> , pages 7035–7052.	822
771	<i>Processing Systems</i> , 35:17359–17372.	Mukund Sundararajan, Ankur Taly, and Qiqi Yan. 2017.	823
772	Kevin Meng, Arnab Sen Sharma, Alex Andonian,	Axiomatic attribution for deep networks. In <i>Internat-</i>	824
773	Yonatan Belinkov, and David Bau. 2022b. Mass-	<i>ional conference on machine learning</i> , pages 3319–	825
774	editing memory in a transformer. <i>arXiv preprint</i>	3328. PMLR.	826
775	<i>arXiv:2210.07229</i> .	Hugo Touvron, Thibaut Lavril, Gautier Izacard, Xavier	827
776	Neel Nanda, Senthooran Rajamanoharan, Janos Kramar,	Martinet, Marie-Anne Lachaux, Timothée Lacroix,	828
777	and Rohin Shah. 2023. Fact finding: Attempting to	Baptiste Rozière, Naman Goyal, Eric Hambro,	829
778	reverse-engineer factual recall on the neuron level.	Faisal Azhar, et al. 2023. Llama: Open and effi-	830
779	In <i>Alignment Forum</i> , page 6.	cient foundation language models. <i>arXiv preprint</i>	831
		<i>arXiv:2302.13971</i> .	832
780	Catherine Olsson, Nelson Elhage, Neel Nanda, Nicholas	Jesse Vig, Sebastian Gehrmann, Yonatan Belinkov,	833
781	Joseph, Nova DasSarma, Tom Henighan, Ben Mann,	Sharon Qian, Daniel Nevo, Yaron Singer, and Stuart	834
782	Amanda Askell, Yuntao Bai, Anna Chen, et al. 2022.	Shieber. 2020. Investigating gender bias in language	835
783	In-context learning and induction heads. <i>arXiv</i>	models using causal mediation analysis. <i>Advances</i>	836
784	<i>preprint arXiv:2209.11895</i> .	<i>in neural information processing systems</i> , 33:12388–	837
785	Long Ouyang, Jeffrey Wu, Xu Jiang, Diogo Almeida,	12401.	838
786	Carroll Wainwright, Pamela Mishkin, Chong Zhang,	Ben Wang and Aran Komatsuzaki. 2021. Gpt-j-6b: A 6	839
787	Sandhini Agarwal, Katarina Slama, Alex Ray, et al.	billion parameter autoregressive language model.	840

841 Kevin Wang, Alexandre Variengien, Arthur Conmy,
842 Buck Shlegeris, and Jacob Steinhardt. 2022. In-
843 terpretability in the wild: a circuit for indirect ob-
844 ject identification in gpt-2 small. *arXiv preprint*
845 *arXiv:2211.00593*.

846 Lean Wang, Lei Li, Damai Dai, Deli Chen, Hao Zhou,
847 Fandong Meng, Jie Zhou, and Xu Sun. 2023. Label
848 words are anchors: An information flow perspective
849 for understanding in-context learning. *arXiv preprint*
850 *arXiv:2305.14160*.

851 Jason Wei, Xuezhi Wang, Dale Schuurmans, Maarten
852 Bosma, Fei Xia, Ed Chi, Quoc V Le, Denny Zhou,
853 et al. 2022. Chain-of-thought prompting elicits rea-
854 soning in large language models. *Advances in neural*
855 *information processing systems*, 35:24824–24837.

856 Zeping Yu and Sophia Ananiadou. 2024. Neuron-
857 level knowledge attribution in large language models.
858 *arXiv preprint arXiv:2312.12141*.

859 Wei Zhang, Wan Chaoqun, Yonggang Zhang, Xinmei
860 Tian, Xu Shen, and Jieping Ye. 2023. Interpreting
861 the inner mechanisms of large language models in
862 mathematical addition.

863 Ziqian Zhong, Ziming Liu, Max Tegmark, and Jacob
864 Andreas. 2024. The clock and the pizza: Two sto-
865 ries in mechanistic explanation of neural networks.
866 *Advances in Neural Information Processing Systems*,
867 36.

A Four Prompts in Arithmetic Dataset

type	prompt
addition-1	The sum of n1 and n2 is
addition-2	Q: What is n1 plus n2? A:
addition-3	n1 plus n2 is
addition-4	n1 + n2 =
subtract-1	The difference between n1 and n2 is
subtract-2	Q: What is n1 minus n2? A:
subtract-3	n1 minus n2 is
subtract-4	n1 - n2 =
multiply-1	The product of n1 and n2 is
multiply-2	Q: What is n1 times n2? A:
multiply-3	n1 times n2 is
multiply-4	n1 * n2 =
division-1	The ratio of n1 and n2 is
division-2	Q: What is n1 divides n2? A:
division-3	n1 divides n2 is
division-4	n1 / n2 =

Table 14: Four prompts for 2-digit arithmetic operations.

B Results of Interventions on Head 14¹⁹

We conduct the same experiments as discussed in Section 4.2-4.4. The results of head 14¹⁹ is shown in Table 15 (corresponding to Table 5), Table 16 (corresponding to Table 6), and Table 17 (corresponding to Table 8).

	top99	top50	top30	top20	top10
mask	84.6	82.1	74.4	66.7	51.3
keep	48.7	51.3	53.9	53.9	64.2
coef	50%	61%	67%	70%	73%

Table 15: Decrease (%) of accuracy and coefficient score on all 1D/ cases when masking and keeping the top FFN neurons.

In Table 15, when head 14¹⁹ is intervened, coefficient scores of important neurons in deep FFN layers are reduced, causing the accuracy decrease. Also, the top identified neurons contain much information. Interventions on top99 neurons result in an accuracy decrease of 84.6%.

	top99	top50	top30	top20	top10
coef	1.3	0.9	3.2	4.9	7.0

Table 16: Decrease (%) of coefficient score when intervening the lowest neuron among important FFN neurons.

The results of Table 16 also demonstrate that among the identified important neurons, the lower neurons can enhance higher neurons' coefficient scores among deep FFN neurons. Therefore, the prediction enhancing stage also exists.

	M=0	M=1	M=2	M=3
number	51,980	10,426	1,953	510
acc	97.5	82.1	30.8	25.7

Table 17: Decrease (%) of accuracy on 1D/ cases when intervening hidden-interpretable neurons.

In Table 17, The hidden-interpretable neurons in shallow FFN layers are important for 1D/ cases (e.g. "72/8="). When intervening 10,426 hidden-interpretable shallow FFN neurons, the accuracy reduces 82.1%. For comparison, we randomly intervene 10,426 FFN neurons in shallow FFN layers, and the interventions only cause a decrease of 5.1%.

Overall, head 14¹⁹ shares the same mechanism with head 17²². Head 14¹⁹ stores important parameters for division operations, while head 17²² is responsible for addition and subtraction.

C Results of Interventions in GPT-J

We conduct the same experiments in Section 3.3 in GPT-J. The accuracy when intervening each head is presented in Table 18.

	ori	7 ⁰	13 ⁹	0 ¹¹	15 ⁶	14 ¹⁴
all	74.5	63.6	64.4	65.0	68.8	70.8
2D+	97.0	95.0	94.0	98.0	95.0	97.0
2D-	78.6	63.6	41.8	63.6	74.5	80.0
2D*	71.0	54.0	72.0	53.0	59.0	72.0
2D/	51.5	42.0	50.0	45.6	46.7	34.4

Table 18: Accuracy (%) when intervening different heads in GPT-J.

In GPT-J, we also observe that different heads store important parameters for various operations. For instance, the accuracy of 2D- decreases significantly when intervening in head 13⁹, whereas head 14¹⁴ holds significant parameters for 2D/.

Then we apply the CNA method between the original model and the intervened model on head 13⁹ on 2D- cases. The results are shown in Table 19 (corresponding to Table 5), Table 20 (corresponding to Table 6), and Table 21 (corresponding to Table 8).

	top99	top50	top30	top20	top10
mask	58.4	45.9	33.4	25	25
keep	37.5	50	54.1	83.4	95.9
coef	17%	20%	21%	23%	29%

Table 19: Decrease (%) of accuracy and coefficient score when masking and keeping the top FFN neurons.

	top99	top50	top30	top20	top10
coef	1.9	1.7	1.6	1.2	1.9

Table 20: Decrease (%) of coefficient score when intervening the lowest neuron among important neurons.

In Table 19, the top FFN neurons also play a large role in GPT-J. When intervening the top99 neurons, the accuracy decreases 58.4%. Compared with Llama, the degrees of coefficient decrease and accuracy change are both smaller. In Table 20, when intervening the lowest neuron among the important neurons identified by our CNA method, the deep neurons’ coefficient scores decrease.

	M=0	M=1	M=2	M=3
number	-	4,272	1,228	564
acc	-	100.0	83.4	20.8

Table 21: Decrease (%) of accuracy when intervening hidden-interpretable neurons.

Results in Table 21 indicate that the hidden-interpretable shallow FFN neurons also exist in GPT-J. When intervening 4,272 neurons, the accuracy decreases 100%.

Overall, we observe similar results in GPT-J. Similar to Llama, GPT-J also exhibits the presence of four stages: feature enhancing, feature transferring, feature predicting, and prediction enhancing.

D Details for Evaluating Gender Bias

We design eight prompts to find the most common professions causing the gender bias. The prompts are shown in Table 22, where <gend> is "man" or "woman".

We compute the top100 predictions of each prompt for different genders, and compare the different professions, which are shown in Table 23. These professions contain much gender bias. We then apply our CNA method between cases with different genders under the first prompt, and identify the top18 important neurons causing the difference. Finally, we edit the top18 neurons by setting their parameters to zero, and then compute the per-

prompt
A <gend> works as a
A <gend> is employed as a
A <gend> holds a job as a
A <gend>’s occupation is
The job of a <gend> is
The work of a <gend> is
The profession of a <gend> is
The work of a <gend> involves

Table 22: Eight prompts for gender bias professions.

plexity difference between different genders for all prompts in both the original and edited model (results are shown in Table 13).

gend	profession
woman	cleaner, nurse, secretary, domestic helper, maid, reception, seller, server, librarian, pharmacist, translator, beautician, dental assistant, hairdresser, volunteer, bookkeeper
man	police, guard, delivery, labour, driver, machinist, roofer, machine operator, lumberjack, technician, miner, night-watch, painter, photographer, builder, porter

Table 23: Professions with gender bias.

E Important Heads for 1-Digit, 2-Digit and 3-Digit Operations

We report the top5 important heads for 1D, 2D and 3D operations in this section. For each operation, the experiments are conducted on the last prompt in Table 14. The results are shown in Table 24-27.

	ori	17 ²²	15 ²³	6 ²⁰	13 ¹⁵	14 ¹⁹
1D+	88.9	47.6	82.8	84.1	84.1	84.1
	ori	17 ²²	15 ⁹	13 ²	6 ²⁰	12 ¹⁶
2D+	94.5	39.3	86.0	87.9	88.6	89.2
	ori	17 ²²	8 ¹⁰	15 ²³	12 ¹⁶	15 ⁹
3D+	96.1	46.4	82.7	83.5	85.2	87.2

Table 24: Results of most important heads for 1D+, 2D+, and 3D+.

	ori	17 ²²	16 ¹	15 ²³	2 ²⁶	13 ²
1D-	82.0	31.0	51.0	53.0	57.0	65.0
	ori	16 ¹	17 ²²	13 ²	15 ²³	12 ¹⁶
2D-	80.0	33.9	37.9	61.8	63.3	70.6
	ori	16 ¹	17 ²²	15 ²³	13 ²	12 ¹⁶
3D-	57.1	19.6	22.9	29.3	34.3	40.7

Table 25: Results of most important heads for 1D-, 2D-, and 3D-.

	ori	3 ⁵	20 ¹⁸	6 ²⁴	17 ²²	0 ³⁰
1D*	93.0	85.4	86.7	87.3	89.2	89.2
	ori	15 ⁹	14 ¹⁹	17 ²²	20 ¹⁸	3 ⁵
2D*	56.9	49.3	50.1	50.5	50.5	51.6
	ori	3 ⁵	15 ⁹	14 ¹⁹	13 ¹⁹	2 ¹⁴
3D*	32.8	25.9	29.7	30.3	31.1	31.1

Table 26: Results of most important heads for 1D*, 2D*, and 3D*.

	ori	14 ¹⁹	15 ⁹	21 ²⁴	6 ²⁴	16 ²¹
1D/	78.9	35.6	61.1	65.6	67.8	68.9
	ori	14 ¹⁹	12 ¹	3 ³	16 ²¹	1 ²⁹
2D/	48.6	13.7	30.2	31.4	36.9	38.8
	ori	14 ¹⁹	3 ³	12 ¹	6 ²²	15 ⁹
3D/	19.0	9.67	12.7	13.0	13.3	13.7

Table 27: Results of most important heads for 1D/, 2D/, and 3D/.